Available online at www.sciencedirect.com
ScienceDirect
Earth and Planetary Science Letters 253 (2007) 445–454
EPSL
www.elsevier.com/locate/epsl

Influence of climate and hydrology on carbon in an early Miocene peatland

Johnny Briggs [a], David J. Large [a,*], Colin Snape [a], Trevor Drage [a], David Whittles [a], Mick Cooper [a], Joe H.S. Macquaker [b], Baruch F. Spiro [c]

[a] School of Chemical, Environmental and Mining Engineering, University of Nottingham, University Park, Nottingham NG7 2RD, UK
[b] Department of Earth Sciences, University of Manchester, Oxford Road, Manchester M13 9PL, UK
[c] Department of Mineralogy, Natural History Museum, Cromwell Road, London SW7 5BD, UK

Received 5 September 2006; received in revised form 31 October 2006; accepted 2 November 2006
Available online 8 December 2006
Editor: M.L. Delaney

Abstract

Our understanding of the hydrodynamic response of peatland to climate change is restricted to the Holocene, which confines our knowledge of the fundamental controls on this important carbon reservoir to recent sedimentary successions. To understand the interaction of peatland hydrodynamics, climate and the carbon cycle on longer time scales, a 95.4 m record from lower Miocene lignite from the Gippsland Basin, Australia is considered. $\delta^{13}C$ and colour records for the lignite were created by analysing samples every 0.1 m. Solid-state ^{13}C NMR results indicate that lignite colour is related to the relative abundance of aliphatic carbon. The lack of a direct correlation between colour and $\delta^{13}C$ demonstrates that the $\delta^{13}C$ signal has not been significantly influenced by the diagenetic processes that produce the colour. An offset correlation occurs between $\delta^{13}C$ and colour with the degree of offset decreasing from 4.5 m at the base to about 0 m at the top. This offset is considered to represent a zone of surface influence that extends up to 20 m below the peat surface. Using numerical modelling we demonstrate that this zone of surface influence and its gradual decline in thickness could arise as a consequence of enhanced fluid flow in regions of high tensile stress within the unconfined peat body. The removal of lignin and its derivatives from the zone of surface influence will be favoured by cooler drier periods, with lower sea level and high hydraulic gradients across the peatland. Therefore in the early Miocene this peatland acted as a carbon source during global cooling.

Keywords: Lignite; Miocene; Carbon; Peatland

1. Introduction

Peatland is a significant carbon reservoir. Northern Hemisphere peatlands contain 455 Gt of carbon [1], approximately one third of the total world soil carbon pool of 1395 Gt [2], and sequester 0.096 Gt C yr^{-1}. As peatland contains 88–97% water [3], predominantly below the thin acrotelm (aerobic and seasonally saturated surface layer above the permanent water table), peatland dynamics are extremely sensitive to changes in the hydrological cycle, which in turn respond to variations in the climate and the carbon cycle. The fact that most peatland carbon is contained within

* Corresponding author.
E-mail address: david.large@nottingham.ac.uk (D.J. Large).

0012-821X/$ - see front matter © 2006 Elsevier B.V. All rights reserved.
doi:10.1016/j.epsl.2006.11.010

postglacial boreal and subarctic peat [1] restricts our understanding of peatland evolution to the high latitudes over periods of <10 kyr [4,5]. In this paper: lignite colour and $\delta^{13}C$ records are used to deduce a link between climate, peatland hydrology and carbon cycling over a period of ca. 1 m.y. in the early Miocene.

2. Geological setting, data and method

The lower Miocene Morwell 1B lignite was deposited in an ombrotrophic peatland environment, in an ocean-margin setting in the Gippsland Basin, Victoria, Australia [6] at a paleolatitude of ~ 50°S [7] (Fig. 1). Initiation of seam formation has been constrained through lithostratigraphic and biostratigraphic parameters as close to the Oligocene/Miocene boundary [6]. Accumulation of a 76 m Morwell 1B colour record [8] has been previously constrained using orbital tuning as between 21.45 and 22.56 Ma [9]. This age is in close agreement with the K/Ar age constraints of contemporaneous volcanics [10]. The seam is up to 120 m thick where it is mined at Loy Yang with no intervening sand or clay partings. The moisture content of the Morwell 1B lignite at Loy Yang is 62.9% [11]. On a dry basis, the average carbon content is 69%, the average ash content is 1.1% and the average specific gravity is 0.76 g/cm^3 [11]. This lignite seam was chosen on account of its ocean-margin setting, thickness and existing age model, all of which should maximise the chance of linking its evolution to changes in global climate.

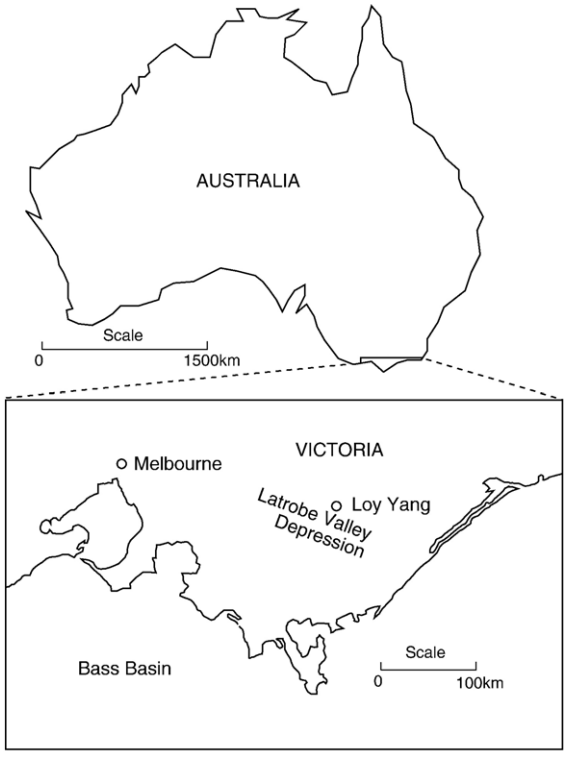

Fig. 1. Location map showing the position of the Loy Yang mine.

Two cores LY4017 (38° 13′ 37.58653″ S, 146° 34′ 41.62420″ E), and LY4018 (38° 13′ 48.03173″ S, 146° 34′ 33.30250″ E) and a set of hand samples were collected from the Loy Yang mine site. These three sets of samples were combined to produce a 95.4 m composite record for the Morwell 1B seam. The hand sample traverse had a 1.2 m overlap with the top of core LY4017 which in turn had a 7.7 m overlap with the top of core LY4018. The composite record was produced using detailed mine plans which constrained the overlap to within 1 m. Fine adjustment to this overlap was made by comparing colour and $\delta^{13}C$ records in the interval of overlap. Individual records and the composite records are provided (Supplementary data). Missing intervals in the data set represent no core recovery.

The lignite colour and $\delta^{13}C$ values of bulk-homogenised lignite were measured from discrete samples collected, where possible, every 0.1 m from 95.4 m of the Morwell 1B seam (Supplementary data). Where observed, fossil wood samples were also collected. All samples were ground and homogenised prior to further treatment. $\delta^{13}C$ analysis was performed on 0.2 mg of sample. Stable carbon isotopic compositions of bulk and whole wood lignite samples were determined by online combustion in a Carlo Erba NA 1500 elemental analyser, coupled via a Con-Flo II interface to a Thermo Finnigan Delta plus XP isotope ratio-mass spectrometer (Thermo Finnigan Corporation, Breman, Germany). Results were reported relative to vPDB with calculated standard deviation of duplicate analysis at 0.06‰. Accuracy was checked using the standard reference material IAEA-CH-7 polyethylene ($\delta^{13}C = -31.8$‰).

Colour measured using the CIE L*A*B* colour scale involves measurement of diffuse reflectance of monochromatic light from a powdered, homogenised and compacted sample undertaken using a Hunterlab Colourflex colorimeter. The L^* value represents the lightness of the material on a linear scale from 0% (black) to 100% (perfect reflecting diffuser), and was selected to represent colour variation of the lignite. L^* was chosen as it was the colour component which displayed the greatest variation.

Solid-state ^{13}C NMR was used to explore the proportion of aliphatic to aromatic carbon and the decay state of lignin. Nine samples were selected for ^{13}C NMR analysis. These samples were chosen to represent the full range of L^* values in the seam. Spectra were

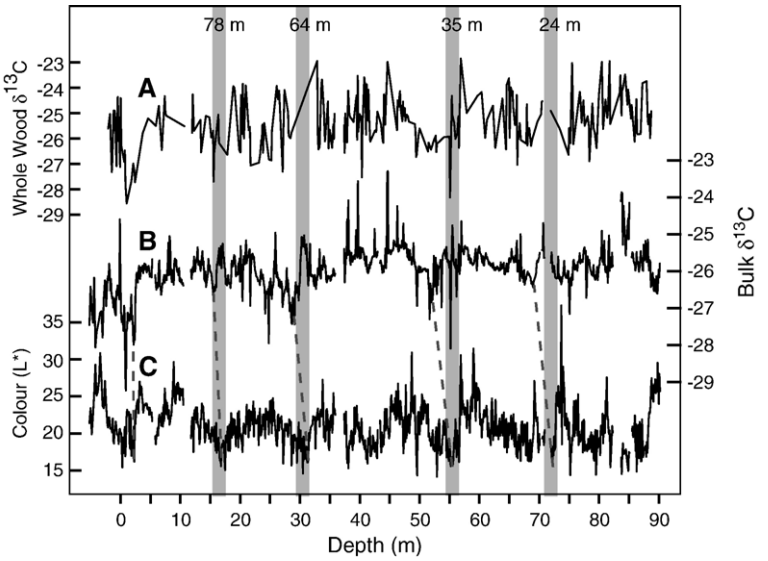

Fig. 2. A) Morwell 1B whole wood δ^{13}C record. B) Morwell 1B bulk δ^{13}C record. C) Morwell 1B L^* record. Lines labelled 24 m, 35 m, 64 m and 78 m are inferred regional disconformities identified by [6] the numerical designation referring to the distance above the base of the Morwell 1B sequence. Correlation points of the inferred lag are indicated by lines connecting the Morwell 1B L^* and δ^{13}C records.

obtained using a Bruker DSX200 instrument equipped with double-bearing probes for cross polarization and magic angle spinning. The resonance frequency for ^{13}C was 5.0 MHz, and the sample was spun at the magic angle with a speed of 5 kHz. The contact time and relaxation delay for cross polarization was 3.0 ms and 1.5 s respectively, with 10 000 scans accumulated for high-power ^{1}H decoupling. All spectra were obtained at ambient temperature and processed with a line-broadening factor of 50 Hz. Chemical shifts were calibrated using an external sample of tetrakis(trimethylsilyl)silane.

An offset correlation between L^* and δ^{13}C was observed (Fig. 2), the degree of offset decreasing gradually from the base to the top of the core. To better constrain this visual observation the following method was applied. The offset producing the maximum positive correlation was estimated every 5 m along the record. The 5 m window length was chosen as this was slightly greater than the visually estimated 4 m offset at the base of the core and less than the scale on which the offset appears to vary. At the base of the core this window length was set at 5.4 m to accommodate the full length of core. For each 5 m window, the correlation coefficient (r) between colour and δ^{13}C was calculated at every 0.1 m up to a total offset of −5.0 m. For example, the L^* values in the depth interval of 85.1 to 90 m were successively correlated with δ^{13}C values in the intervals 85.1–90 m (0 m offset), 85–89.9 m (−0.1 m offset), 84.9–89.8 m (−0.2 m offset) ….. 80.1–85.0 m (−5.0 m offset). A graph of offset vs r was then plotted for each 5 m interval and the offset that gave the maximum positive r value noted. Only graphs that gave a distinct maximum r value were used. Maximum r values were generally in the range from 0.4 to 0.8, $p<0.020$.

In order to position the Morwell 1B lignite within a global and temporal framework, it was necessary to convert depth to time. The δ^{13}C record was positioned in accordance with an existing age model [9]. This position was then refined by tuning an inferred ca. 100 kyr eccentricity signal in the lignite δ^{13}C record to the ca. 100 kyr eccentricity signal isolated from the orbitally tuned marine benthic foraminiferal δ^{13}C record [12]. Eccentricity components were isolated in both records using singular spectrum analysis [13]. Prior to singular spectrum analysis the data was resampled every 0.1 m using a constrained cubic spline. Based on previous work on the Morwell seam [9] the eccentricity signal in the lignite was expected at about 0.11 cycles/m. The inferred eccentricity signal identified by SSA occurred at 0.12 cycles/m, similar to the expected value. The revised tuning indicates that the Morwell 1B at Loy Yang formed between 21.55 and 22.81 Ma (Fig. 3). Within this time interval both the marine and lignite records display similar long term trends and shorter term variations (Fig. 3).

3. Results and observations

Bulk δ^{13}C values (Fig. 2) vary from −29.2‰ to −23.2‰ with an average carbon isotope composition of

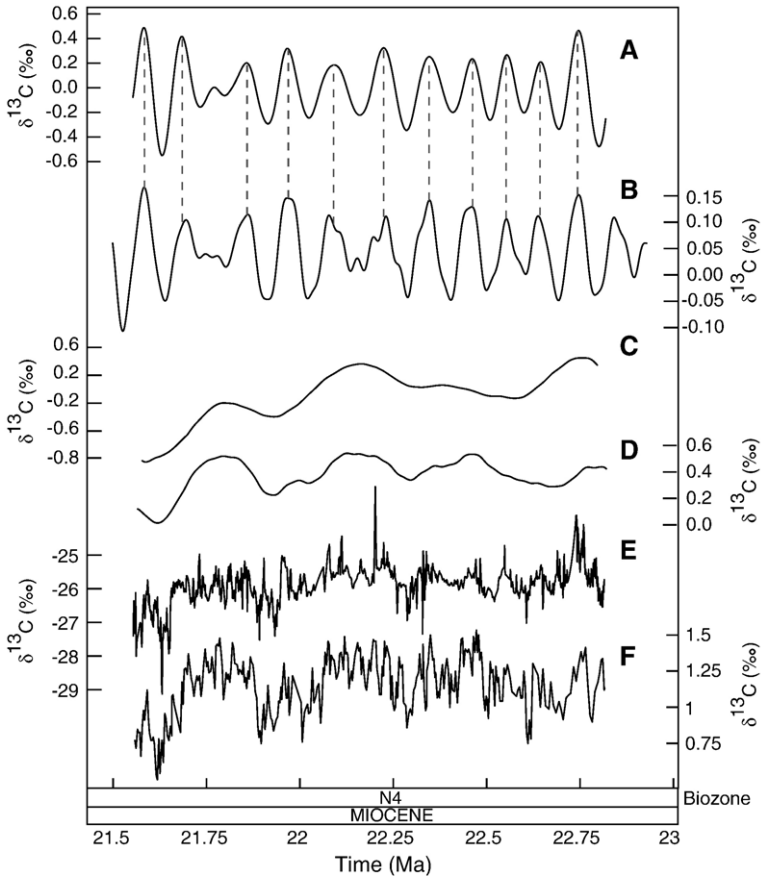

Fig. 3. A) Tuned ca. 100 kyr eccentricity signal from the Morwell 1B δ^{13}C record. B) ca. 100 kyr eccentricity signal derived from the marine ODP site 926/929 δ^{13}C record [12], 21.5–23 Ma. C) Tuned background trend of the Morwell 1B δ^{13}C record. D) Background trend of the marine ODP site 926/929 δ^{13}C record [12]. Signals within A, B, C and D identified and plotted by using singular spectrum analysis [13]. E) Tuned Morwell 1B δ^{13}C record. F) Marine ODP site 926/929 δ^{13}C record [12], 21.55–22.81 Ma.

−25.9‰. This range is typical for C3 plants. δ^{13}C values of wood separates vary from −28.6‰ to −22.9‰ with an average of −25.4‰, significantly ($p<0.001$) more ^{13}C enriched than the respective bulk samples. However, records of wood and bulk samples display similar trends ($r=0.77$, $p<0.001$). The long term trend in δ^{13}C is a general decrease up section and is similar to that observed in contemporaneous marine benthic foraminiferal δ^{13}C record (Fig. 3).

Over the entire profile the average L^* value increases from the base to the top by about 3 units, with an overall range of 23 units. L^* values display lightening-up cycles that correspond to those observed in regionally correlated Colour Index records, a major component of which is lightness [8,10,14]. Each cycle begins with a dark coal and gradually lightens upward before abruptly darkening, creating in places an asymmetrical saw-tooth profile. Abrupt transitions from light to dark have been interpreted as regional disconformities [6]. In the field, the contact between light and dark lithotypes is sometimes undulating, with a relief of up to 0.5 m and accompanied by small amounts of charcoal (Fig. 4). Charcoal is thickest at the base of the undulations, thins over highs, and in places intrudes into the underlying pale lignite (Fig. 4).

Results of solid-state ^{13}C NMR (Fig. 5) indicate that the proportion of aromatic to aliphatic carbon correlates with L^* ($r=0.9$, $p<0.001$) but not with δ^{13}C ($r=0.046$). As L^* increases sharp peaks characteristic of lignin disappear indicating that lignin becomes more degraded as the proportion of aliphatic carbon increases.

Comparison between entire δ^{13}C and L^* records shows no direct correlation ($r=0.08$). However, both data sets tend to display similar, though not identical trends, on scales of 15 to 30 m. These trends appear to be offset with changes in colour occurring temporally before the corresponding changes in δ^{13}C and this offset between the records appears to decrease upwards (Fig. 2). The

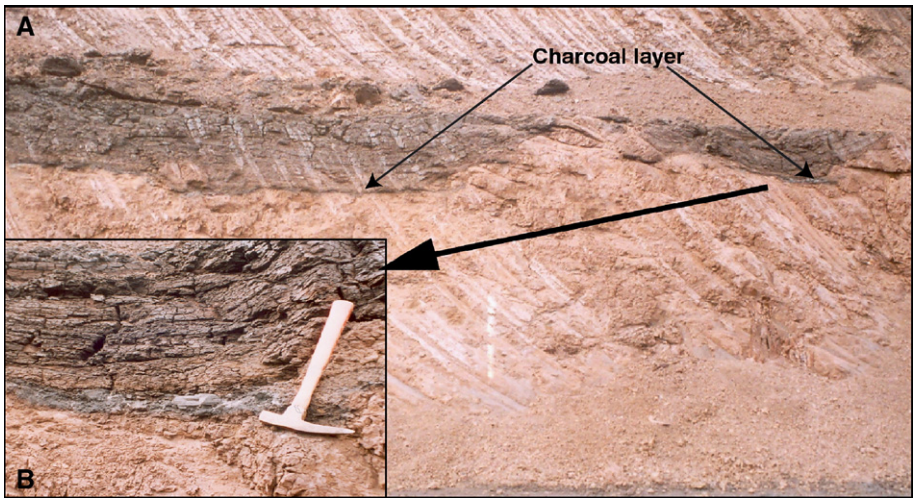

Fig. 4. A) Undulating contact between light and dark lithotypes in the Morwell 1B seam. A dark charcoal layer occurs at the contact, thickens within troughs and is thin or absent over crests. B) Close up view of the thick charcoal layer in the trough.

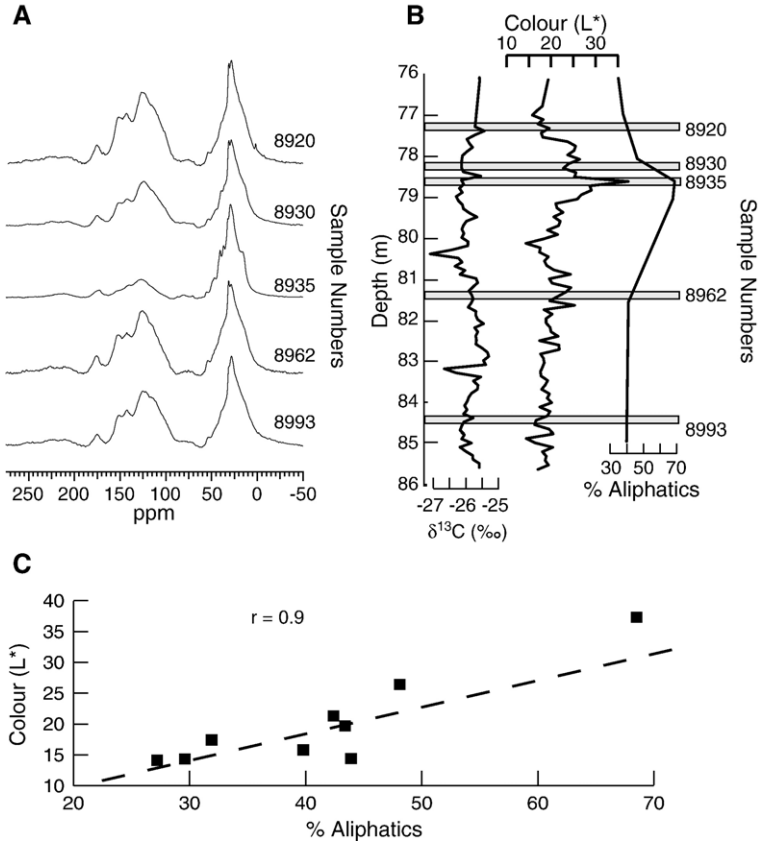

Fig. 5. Detailed presentation of parameters measured on peat samples from a full lightening upwards cycle, 77.4 to 84.7 m. A) Solid-state ^{13}C CP/MAS NMR spectra from selected samples in a lightening upward sequence. B) Comparison of corresponding $\delta^{13}C$ and colour values with % aliphatics taken as a % total carbon value from within the 0–50 ppm range (in A). C) Plot of colour (L^*) versus % aliphatics includes 4 other samples tested but not included on A and B.

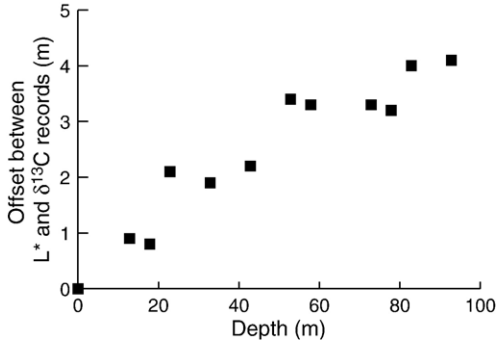

Fig. 6. Estimate of offset between $\delta^{13}C$ and L^* plotted against depth. Details of how the offset is estimated are given in the methods section.

graph of offset vs depth (Fig. 6) demonstrates that the offset decreases from approximately 4.5 m at base of the record to 0 m at the top.

4. Discussion

4.1. Interpretation of L^* and $\delta^{13}C$

To understand the evolution of the peatland it is first necessary to decide what interpretation can be placed on the two proxies L^* and $\delta^{13}C$. Lignite colour is primarily a response to the conditions that govern decay [15]. This interpretation is consistent with the observed correlation between the percentage of aliphatic carbon and L^*. Such large changes in the total amount of aliphatic carbon in terrestrially derived organic matter can only be accounted for by the preferential decay and removal of non-aliphatic carbon. The lighter coloured samples with higher L^* values are therefore more decayed.

The positive correlation of $\delta^{13}C$ data of bulk and wood separates, and the lack of direct correlation to colour and aliphatic abundance, indicates that changes in the $\delta^{13}C$ of both bulk and wood samples are strongly influenced by the isotopic variability of the original plant matter and not by diagenetic processes. The $\delta^{13}C$ record will therefore provide a time integrated measure of changes in the balance between CO_2 uptake and water loss, after accounting for changes in the $\delta^{13}C$ of atmospheric CO_2 [16]. The deviation of the bulk $\delta^{13}C$ data towards lighter values than the wood separates is most likely due to the increased presence of isotopically light leaves, resins and bark in the lignite matrix [17], or a greater representation of isotopically lighter angiosperm shrub vegetation [18] in the bulk lignite.

To evaluate the degree to which the $\delta^{13}C$ of atmospheric carbon has influenced the lignite $\delta^{13}C$, the lignite record was compared to a contemporaneous marine benthic foraminiferal $\delta^{13}C$ record (Fig. 3). Correlation was established using an existing orbital tuning of oscillations within the Morwell seam colour record to the theoretical insulation curve [9]. Both records display evidence of similar long term (approximately 400 and 100 kyr) oscillations and a general decrease in $\delta^{13}C$ of the exogenic carbon reservoir between 22.6 and 21.5 Ma. Evidence for covariance between marine benthic foraminiferal $\delta^{18}O$ and $\delta^{13}C$ values at low frequencies during the Early Miocene [19] indicate ocean/atmospheric ^{13}C enrichment is associated with global cooling and vice versa. It is therefore likely that the long term trends in the lignite $\delta^{13}C$ record are responding to the same processes. However, the $\delta^{13}C$ trend recorded in the lignite is amplified by a factor of approximately 3 relative to the marine record.

This implies that there must have been some ecophysiological adaptation of terrestrial plants imprinted upon changing atmospheric $\delta^{13}C$ in order to account for the amplified isotopic fractionation [20,21] In the absence of any clear relationship to the decay processes operating in the peat, the most likely means of achieving this amplification is through temperature variation, relative humidity and soil water availability which set the level of water stress [20]. Plants respond to water stress by closing their stomata [22], this in turn leads to ^{13}C enrichment [23]. Long term increases in $\delta^{13}C$ may therefore correspond to relatively cooler and drier periods with decreased discrimination against ^{13}C.

The correspondence of cooler with drier and warmer with wetter may reflect the relationship between global temperature, soil moisture and the concentration of atmospheric CO_2. In particular it has been shown that the increase in atmospheric CO_2 accompanying global warming has suppressed plant transpiration increasing soil moisture and runoff [24] with the opposite expected during periods of cooling and decreasing CO_2. As changes in soil moisture, even in relatively wet soils, will result in changes in water stress and isotope discrimination [20] this provides a mechanism whereby change in temperature can be coupled to changes in soil moisture via the carbon cycle.

Another mechanism affecting soil moisture that is strongly coupled to global temperature is changing sea level. During cool periods, with enhanced ice formation and low sea levels, hydraulic gradients will increase across the peatland and water tables should fall producing a drier soil [25]. It is not possible to say which of these is likely to be the strongest influence but in general cooler periods are likely to be accompanied by drier peatlands due to either enhanced transpiration, lower sea level or both, with the opposite applying during warmer intervals.

4.2. Interpretation of the offset between L^* and $\delta^{13}C$

The offset correlation between L^* and $\delta^{13}C$ indicates that there is a common influence on the processes that determine carbon exchange between plant matter and the atmosphere and the subsequent decay processes at various depths in a zone of surface influence within the peat.

The slight, 3 unit, increase in L^* that accompanies the decrease in offset over the entire seam is small compared to shorter term changes in L^* (10–15 units), and within a single lightening upward cycle there is no discernable variation in offset. This indicates that the colour is not directly proportional to the offset. We therefore propose that colour depends not on the residence time in the zone of surface influence or its thickness but on the intensity of some surface driven process within this zone.

The depth to which surface processes influenced peat composition can be judged from the scale of the offset correlation. Assuming near surface dry peat densities similar to those in tropical peat of 0.175 g cm^{-3} [26] and an average dry density of the Morwell 1B lignite of 0.63 g/cm^3 [9] then surface processes must have influenced the peat to a depth of at least 15 to 20 m at the base of the seam. A zone of surface influence this thick is not analogous to the acrotelm which rarely exceeds depths of more than a few tens of centimetres in modern pristine peat [27]. So some mechanism is required by which climate driven surface processes can influence the peat to depths of at least 20 m deep and the thickness of this zone of surface influence must decrease as the peat accumulates.

Near surface processes within the peat must also play a role in determining colour. Evidence of this is the rapid transition from light to dark lithotypes accompanied by an undulating surface and charcoal. We interpret this association as evidence of subsurface and surface burning of the peat followed by collapse of the peat surface. This interpretation is consistent with the observed increase in the thickness of charcoal under topographically low points on the contact. Using the same densities to those used above, the relief at these contacts is unlikely to represent more than 2 m of peat loss. As burning requires both oxygen and relatively dry peat, such a process must occur in the near surface and this process is also related to a change in colour.

4.3. Mechanisms explaining the offset

Three inter-related processes are required to explain the offset: a means of systematically decreasing the zone of surface influence as the seam accumulates; a mechanism whereby changes in surface processes can influence the peat to depths possibly exceeding 20 m; a process for removing aromatic carbon.

A possible cause of the zone of surface influence and its subsequent decrease in thickness as the peat accumulates is the height of peat above some base level. This can be demonstrated using models of Holocene peat growth [28,29]. In these models the rate at which peat grows is a balance between the input to the saturated peat and the rate of decay in the bulk of the peat. As the total thickness of peat increases the mass lost increasingly balances the input. Using a linear decay model with estimated Holocene values for input and decay [29] the effect of peat growth relative to accommodation below a base level by constant subsidence can be demonstrated (Fig. 7). The height of the peat above base level quickly reaches a maximum and then declines more gradually until the peat surface falls below base level. The underlying principle that input to the peat is gradually balanced by decay determines the basic style of the peat growth curve with peat accumulating at an ever decreasing rate. Whether the Holocene decay model, decay constants and estimated input are correct on longer time scales is questionable but this will not affect the basic style of the curve.

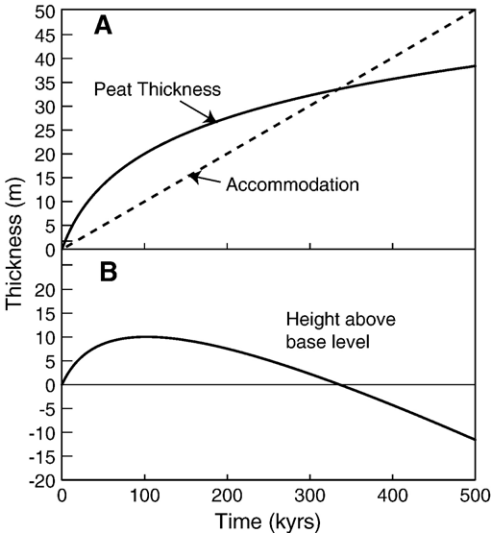

Fig. 7. A) Peat growth vs accommodation curves. The peat growth curve was calculated using a linear growth model $M=p/a.\ \ln(1+aT)$ where M is the mass of carbon accumulated, p is the input 0.002 kg C m^{-2} yr^{-1}, a is the linear decay constant 3.71×10^{-5} yr^{-1} and T is time. Mass of carbon was converted to thickness using a dry density of 0.1 g cm^{-3} and a carbon concentration of 50% w/w. The accommodation curve is calculate using a constant accommodation rate of 0.1 mm yr^{-1}. B) Height above base level calculated by subtracting the accommodation curve from the peat growth curve.

So if this is the case, why would the height of the peat above a base level influence the connectivity of the peat close to base level with the surface? What we propose is that the easiest way to connect surface processes to deeper parts of the peat is by fluid flow and that significant fluid flow can occur only in the near surface unconfined peat close to or above base level due to high tensile stress maintaining high porosity and permeability. From this mechanical view point, base level is defined as the depth below which the peat body is confined by adjacent sediments. During the early stages of peat formation, surface controlled processes successively overprint the colour record as the zone of surface influence increases in proportion to height above base level. At some stage during peat growth overprinting ceases and colour changes produced in the zone of surface influence are continuously preserved. The thickness of this zone of surface influence then gradually diminishes in proportion to the height above base level. In the lignite the point at which overprinting ceases is 4.5 m above the base of the seam [9], which on the calibrated timescale is about 63 kyr after deposition commenced.

To investigate the stresses that develop within a raised peat bog a two dimensional plane strain geomechanical computational model of a, hypothetical, elliptical raised peat bog was constructed. The elliptical shape of the surface is in line with predicted hydrological shape of small raised bogs [30]. The modelling was undertaken using a commercial modelling application (FLAC) which undertakes mechanical calculations using the explicit finite difference method. The two dimensional computer model represented the bog as a two phase peat–water material. Flow of the water within the bog was simulated by a finite difference time stepping form of Darcy's Flow Law. Although water flow in peat is not strictly Darcian reasonable alternatives were not available and Darcian flow is considered a good approximation [31]. The development of mechanical stress and strain within the peat was simulated by a finite difference form of Newton's 2nd Law. The peat itself was modelled as an elastic medium. Coupling between the fluid and solid phases allowed the pore pressures developed within the fluid to be applied as mechanical stresses to the peat during the simulation.

Along the top surface of the bog the pore pressure was fixed at zero and the saturation was allowed to vary. This is the usual boundary condition for a free surface as fluid is allowed to flow to and from the outside world. The base and sides of the bog were represented as impermeable boundaries. The bog was simulated as being initially fully saturated. The material properties adopted within the computational models are shown in Table 1. The hypothetical raised peat bog was represented as a 1 km region of raised peat, reaching a height of 7 m above base level at its centre. Results (Fig. 8) show that tensile stresses occur in the upper raised part of the peat body with a distinct layer of tensile stress just below base level (Fig. 8). So the greatest potential for high porosity enhanced by tensile stress occurs within or immediately below the unconfined upper part of the peat. On the peat surface tensile and compressive stresses alternate in a manner similar to the hummocks and hollows observed on many raised peatlands [32] and this may be a potential mechanism for producing the undulating surface at the contact between light and dark lithotypes. It was not possible to consider the effect of compaction on permeability in this model, however studies of wood tropical peat indicate that there is very little compaction to depths of 8 m, so this may not be a major issue [26].

Table 1

	Water	Peat
Density	1000 kg/m^3	75 kg/m^3
Bulk modulus	2×10^7 N/m^2	2000 N/m^2
Shear modulus	0	1045 N/m^2
Permeability	–	5×10^{-7} m^2/pa s
Porosity	–	80%

The potential for fluid flow will then depend on the permeability of the peat and this may well be a function of aerobic decay processes and the time spent within the acrotelm. Rapid transfer into the saturated layer will promote lignin preservation and gelification [15] and hence low permeability peat, whereas high degrees of aerobic decay will result in a less gelified more permeable peat which can be further leached by deep fluid flow. Recent observations of fluid flow in peatland support the importance of deep fluid flow via pipes and macropores in connecting surface fluids with deep peat [33,34] and this coupled with mechanisms like the enzyme latch [35] may promote deep fluid flow and lignin oxidation even under mildly anaerobic conditions.

Optimal leaching of lignin derivatives from the deep peat will be promoted by steep hydraulic gradients through peat that has previously experienced aerobic decay. A drier climate, coupled to falling sea level would promote higher permeability and steeper hydraulic gradients across the peatland and so would be the optimal conditions for carbon leaching. This requirement is consistent with the inferred coupling of increased water stress with increasing δ^{13}C of

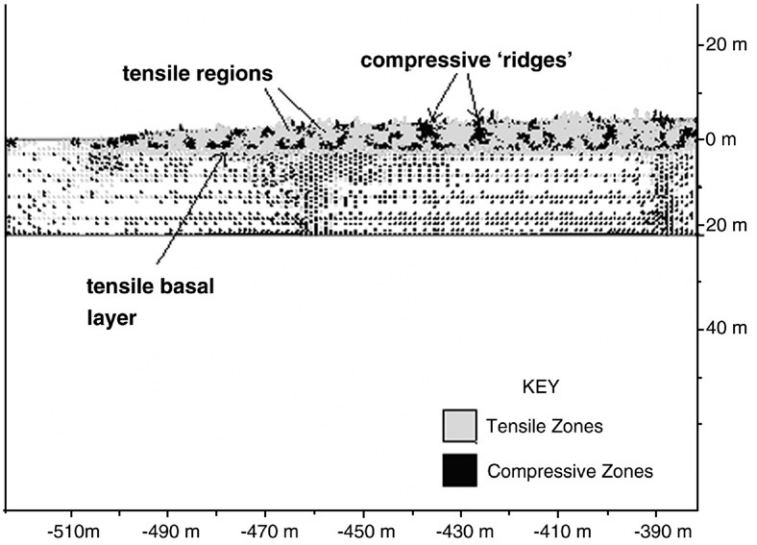

Fig. 8. Model of the distribution of tensile and compressive stress within a raised peatland. Areas of maximum tensile stress are likely to experience enhanced porosity and permeability.

atmospheric carbon which is in turn related to oceanic cooling, ice-sheet expansion and sea level fall [19].

5. Conclusions

If this interpretation is correct then the colour of the peat results from both near surface processes which influence the permeability and porosity of the peat and deeper fluid flow which determines the degradation and removal of lignin derived carbon.

The paler lithotypes that correlate with periods of ^{13}C enrichment therefore most likely correspond to cooling and drying of the peatland with subsequent deep fluid flow and leaching of organic carbon. The additional enrichment in ^{13}C over and above that observed in the marine record is consistent with drier conditions and either water stress induced changes in the ^{13}C discrimination of individual species or the development of a more water stress tolerant plant community [21].

The darker lithotypes will correlate with ^{13}C depletion, warmer wetter conditions with subsequently impaired deep fluid flow and lower hydraulic gradients during periods of higher sea level. The increased discrimination against ^{13}C is consistent with warmer wetter conditions.

If global cooling is associated with increases in marine benthic foraminiferal $\delta^{13}C$ and is in turn a function of changes in atmospheric CO_2 then the peatlands have been acting as carbon sources during cool periods with lower concentrations of atmospheric CO_2, and carbon sinks during warmer periods with higher concentrations of atmospheric CO_2. This peatland will have acted as a negative feedback in the ocean atmosphere system which is markedly different from the present day where increasing CO_2 and global warming are predicted to result in drying of the boreal peatland with the potentially catastrophic loss of carbon producing a positive feedback.

Acknowledgements

This work was supported by the Natural Environmental Research Council Grant NE/C513585/1 and Rio Tinto Technology Development. JB would like to acknowledge the support of Basil Johns and Universitas 21 Scholarship. We wish to thank the editor and two anonymous reviewers, for a speedy and constructive assessment of the manuscript.

Appendix A. Supplementary data

Supplementary data associated with this article can be found, in the online version, at doi:10.1016/j.epsl.2006.11.010.

References

[1] E. Gorham, Northern peatlands — role in the carbon-cycle and probable responses to climatic warming, Ecol. Appl. 1 (2) (1991) 182–195.
[2] W.M. Post, et al., Soil carbon pools and world life zones, Nature 298 (1982) 156–159.
[3] D. Charman, Peatlands and Environmental Change, John Wiley and Sons, Chichester, 2002.

[4] K.V. Kremenetski, et al., Peatlands of the Western Siberian lowlands: current knowledge on zonation, carbon content and Late Quaternary history, Quat. Sci. Rev. 22 (5–7) (2003) 703–723.
[5] D.H. Vitt, et al., Spatial and temporal trends in carbon storage of peatlands of continental western Canada through the Holocene, Can. J. Earth Sci. 37 (5) (2000) 683–693.
[6] G.R. Holdgate, A.P. Kershaw, I.R.K. Sluiter, Sequence stratigraphic analysis and the origins of Tertiary brown coal lithotypes, Latrobe Valley, Gippsland Basin, Australia, Int. J. Coal Geol. 28 (2/4) (1995) 249.
[7] L.A. Lawver, L.M. Gahagan, Evolution of Cenozoic seaways in the circum-Antarctic region, Palaeogeogr. Palaeoclimatol. Palaeoecol. 198 (1–2) (2003) 11–37.
[8] G.H. Mackay, et al., The Cyclic Occurrence of Brown Coal Lithotypes, State Electricity Commission of Victoria, Research and Development Department, 1985, pp. 1–7.
[9] D.J. Large, et al., Orbital tuning and correlation of 1.7 my of continuous carbon storage in an early Miocene peatland, Geology 32 (10) (2004) 873–876.
[10] G.R. Holdgate, The influence of sea-level changes on coal seam deposition and equivalent facies, onshore Gippsland basin, 1996, PhD thesis, Department of Earth Sciences, Monash University, Melbourne.
[11] A.M. George, G.H. Mackay, Petrology, in: R.A. Durie (Ed.), The Science of Victorian Brown Coal: Structure, Properties and Consequences for Utilization, Heinemann, Butterworth, 1991, pp. 45–102.
[12] J. Zachos, et al., Trends, rhythms, and aberrations in global climate 65 Ma to present, Science 292 (5517) (2001) 686–693.
[13] M. Ghil, et al., Advanced spectral methods for climatic time series, Rev. Geophys. 40 (1) (2002).
[14] D.J. Allardice, et al., The Properties of Brown Coals from the Latrobe Valley — Results of Analysis and Tests, State Electricity Commission of Victoria, Research and Development Department Report, 1978.
[15] C.F.K. Diessel, Coal Bearing Depositional Systems, Springer–Verlag, Berlin, 1992.
[16] D.J. Beerling, Ecophysiological responses of woody plants to past CO_2 concentrations, Tree Physiol. 16 (4) (1996) 389–396.
[17] R. Park, S. Epstein, Metabolic fractionation of C^{13} and C^{12} in plants, Plant Physiol. 36 (2) (1961) 133.
[18] A. Lucke, et al., Environmental history of the German Lower Rhine embayment during the Middle Miocene as reflected by carbon isotopes in brown coal, Palaeogeogr. Palaeoclimatol. Palaeoecol. 154 (4) (1999) 339–352.
[19] H.A. Paul, et al., Orbitally induced climate and geochemical variability across the Oligocene/Miocene boundary, Paleoceanography 15 (5) (2000) 471–485.
[20] G.J. Bowen, et al., A humid climate state during the Palaeocene/Eocene thermal maximum, Nature 432 (7016) (2004) 495–499.
[21] N.C. Arens, A. Hope Jahren, R. Amundson, Can C3 plants faithfully record the carbon isotopic composition of atmospheric carbon dioxide? Paleobiology 26 (1) (2000) 137–164.
[22] J.R. Ehleringer, T.E. Cerling, M.D. Dearing, Atmospheric CO_2 as a global change driver influencing plant-animal interactions, Integr. Comp. Biol. 42 (3) (2002) 424–430.
[23] G.D. Farquhar, J.R. Ehleringer, K.T. Hubick, Carbon isotope discrimination and photosynthesis, Annu. Rev. Plant Physiol. Plant Mol. Biol. 40 (1989) 503–537.
[24] N. Gedney, et al., Detection of a direct carbon dioxide effect in continental river runoff records, Nature 439 (7078) (2006) 835–838.
[25] R. Davies, et al., High-resolution sequence-stratigraphic correlation between shallow-marine and terrestrial strata: examples from the Sunnyside Member of the Cretaceous Blackhawk Formation Book Cliffs eastern Utah, AAPG Bull. 90 (7) (2006) 1121–1140.
[26] S.E. Page, et al., A record of Late Pleistocene and Holocene carbon accumulation and climate change from an equatorial peat bog (Kalimantan, Indonesia): implications for past, present and future carbon dynamics, J. Quat. Sci. 19 (7) (2004) 625–635.
[27] Z.C. Yu, et al., Modelling long-term peatland dynamics. II. Processes and rates as inferred from litter and peat-core data, Ecol. Model. 145 (2–3) (2001) 159–173.
[28] R.S. Clymo, The limits to peat bog growth, Philos. Trans. R. Soc. Lond., B Biol. Sci. 303 (1117) (1984) 605–654.
[29] R.S. Clymo, J. Turunen, K. Tolonen, Carbon accumulation in peatland, Oikos 81 (2) (1998) 368–388.
[30] H.A.P. Ingram, Size and shape in raised mire ecosystems: a geophysical model, Nature 297 (1982) 300–303.
[31] H.F. Hemond, J.C. Goldman, On non-Darcian water-flow in peat, J. Ecol. 73 (2) (1985) 579–584.
[32] L.R. Belyea, R.S. Clymo, Feedback control of the rate of peat formation, Proc. - Royal Soc., Biol. Sci. 268 (1473) (2001) 1315–1321.
[33] J. Holden, Controls of soil pipe frequency in upland blanket peat, J. Geophys. Res. –Earth Surf. 110 (F1) (2005).
[34] C.B. Crouse, et al., Dynamic tests of pipe pile in saturated peat, J. Geotech. Eng. — ASCE 119 (10) (1993) 1550–1567.
[35] C. Freeman, N. Ostle, H. Kang, An enzymic 'latch' on a global carbon store — a shortage of oxygen locks up carbon in peatlands by restraining a single enzyme, Nature 409 (6817) (2001) 149.